PERMAFROST AND PERIGLACIAL PROCESSES
Permafrost and Periglac. Process. (2016)
Published online in Wiley Online Library
(wileyonlinelibrary.com) DOI: 10.1002/ppp.1893

Surface Geophysical Methods for Characterising Frozen Ground in Transitional Permafrost Landscapes

Martin A. Briggs,[1]* *Seth Campbell,*[2] *Jay Nolan,*[3] *Michelle A. Walvoord,*[4] *Dimitrios Ntarlagiannis,*[3] *Frederick D. Day-Lewis*[1] *and John W. Lane*[1]

[1] US Geological Survey, Office of Groundwater, Branch of Geophysics, Storrs, CT, USA
[2] Cold Regions Research and Engineering Laboratory, Hanover, NH, USA
[3] Department of Earth and Environmental Sciences, Rutgers - The State University, Newark, NJ, USA
[4] US Geological Survey, National Research Program, Denver Federal Center, Denver, CO, USA

ABSTRACT

The distribution of shallow frozen ground is paramount to research in cold regions, and is subject to temporal and spatial changes influenced by climate, landscape disturbance and ecosystem succession. Remote sensing from airborne and satellite platforms is increasing our understanding of landscape-scale permafrost distribution, but typically lacks the resolution to characterise finer-scale processes and phenomena, which are better captured by integrated surface geophysical methods. Here, we demonstrate the use of electrical resistivity imaging (ERI), electromagnetic induction (EMI), ground penetrating radar (GPR) and infrared imaging over multiple summer field seasons around the highly dynamic Twelvemile Lake, Yukon Flats, central Alaska, USA. Twelvemile Lake has generally receded in the past 30 yr, allowing permafrost aggradation in the receded margins, resulting in a mosaic of transient frozen ground adjacent to thick, older permafrost outside the original lakebed. ERI and EMI best evaluated the thickness of shallow, thin permafrost aggradation, which was not clear from frost probing or GPR surveys. GPR most precisely estimated the depth of the active layer, which forward electrical resistivity modelling indicated to be a difficult target for electrical methods, but could be more tractable in time-lapse mode. Infrared imaging of freshly dug soil pit walls captured active-layer thermal gradients at unprecedented resolution, which may be useful in calibrating emerging numerical models. GPR and EMI were able to cover landscape scales (several kilometres) efficiently, and new analysis software showcased here yields calibrated EMI data that reveal the complicated distribution of shallow permafrost in a transitional landscape. Copyright © 2016 John Wiley & Sons, Ltd.

KEY WORDS: electromagnetic induction; electrical resistivity; geophysics; ground penetrating radar; thermal infrared; permafrost aggradation

INTRODUCTION

In Arctic regions, shallow permafrost and seasonal frozen ground influence the routing and distribution of water above and below the land surface. Characterisation of the active layer is critical for many cold region studies because most subsurface biological, biogeochemical, ecological and pedogenic activity in permafrost regions occurs in this shallow zone. As such, mapping shallow permafrost and monitoring the active layer have been a priority for high-latitude research for the past several decades, particularly given the regional-scale landscape transitions of frozen ground distribution in response to climate warming. Development of the Circumpolar Active Layer Monitoring (CALM) network began in the 1990s and now (Jones, 1999) includes more than 125 sites globally (http://www.gwu.edu/~calm). Remote sensing information has been used to extrapolate point-scale measurements of active-layer thickness (ALT) using empirical and statistical approaches (e.g. Shiklomanov and Nelson, 1999; Pastick *et al*., 2013, 2014). Landscape-scale estimation of ALT has also been accomplished via equilibrium and transient thermal modelling (Riseborough *et al*., 2008, and references therein; Jafarov *et al*., 2012). However, since the depth and distribution of shallow permafrost are influenced by interrelated factors such as surface temperature cycles, thermal and hydrologic properties of surface cover and substrate, soil moisture and soil water fluxes, vegetation and snow cover (Shur and Jorgenson, 2007), fine-scale

* Correspondence to: M. A. Briggs, US Geological Survey, Office of Groundwater, Branch of Geophysics, 11 Sherman Place, Unit 5015, Storrs, CT 06269, USA. E-mail: mbriggs@usgs.gov

Received 20 April 2015
Revised 25 September 2015
Accepted 25 December 2015

patterns and transient features of frozen ground (i.e. the 'transition zone' in Shur *et al.*, 2005) are not represented in these landscape-scale characterisation approaches. Geophysical methods of subsurface characterisation can provide detailed spatial (both lateral and vertical) and temporal information on shallow ground-ice distribution crucial for understanding seasonal dynamics, interannual variability and other long-term transient features reflecting permafrost thaw and aggradation.

Changes in ALT and shallow permafrost (thaw or aggradation) may be expected in response to fire (Johnstone *et al.*, 2010; Jafarov *et al.*, 2013; Jiang *et al.*, 2015), climate (Jorgenson *et al.*, 2010; Jafarov *et al.*, 2012), shifts in vegetation and snow cover (Shur and Jorgenson, 2007), and surface water redistribution (Briggs *et al.*, 2014). Collectively, these changes in the subsurface soil temperature and cryologic regime impact greenhouse gas exchange (Schuur *et al.*, 2015), subsurface flow and transport (Frampton *et al.*, 2012; Wellman *et al.*, 2013), and habitat for wildlife and migratory waterfowl (Prowse *et al.*, 2010). High-resolution, spatially distributed determination of shallow frozen ground is needed for providing the foundation of process-based hydrological, biogeochemical and ecological studies.

Physical methods deployed from the ground surface (e.g. pits, augers, frost probes) can provide precise point-in-time ALTs, but assessing the thickness of frozen ground is difficult. Handheld geophysical approaches in cold regions provide a bridge between point-scale measurements and landscape-scale statistical-empirical or thermal modelling of shallow frozen ground and permafrost. Here, we present a multi-year case study that demonstrates the use of a suite of complementary ground-based geophysical techniques to assess dynamic shallow ground-ice and permafrost distribution in a boreal lowland lake watershed in the Yukon Flats of interior Alaska. This approach offers new insight on multi-method design for capturing fine-scale features of frozen ground in regions that are undergoing transitions involving permafrost thaw and aggradation.

STUDY AREA

Located 13 km south of the Arctic Circle, Twelvemile Lake in the Yukon Flats of interior Alaska has been a site of recent intensive field and modelling investigations aimed at better understanding the interactions between permafrost, groundwater flow and surface water in discontinuous permafrost lowlands (Wellman *et al.*, 2013; Jepsen *et al.*, 2013a, 2013b). Until recently, Twelvemile Lake had been rapidly and steadily declining in lake level and shrinking in surface area since the mid-1970s (Jepsen *et al.*, 2013a). Current investigations suggest that Twelvemile Lake is periodically recharged by upgradient flooding events (e.g. ice jams during spring ice breakup of the Yukon River), resulting in sharp increases (highstands) in lake-level elevation and surface area. Following these episodic lake recharge events, the evaporative demands of the Twelvemile Lake water budget exceed seasonal inputs, resulting in a steady decline in lake level of ~ 0.13 m yr^{-1} and a corresponding reduction in surface area (Jepsen *et al.*, 2013b). Twelvemile Lake's highstand boundary is bordered in places by mature forest dominated by spruce that is underlain by thick (approximately 90 m) permafrost, as evaluated by airborne electromagnetic induction (EMI) survey (Minsley *et al.*, 2012a) and supported by coupled fluid flow and heat transport modelling (Wellman *et al.*, 2013). In contrast to the surrounding forest, areas within the lake highstand perimeter are free of thick permafrost (Minsley *et al.*, 2012a) due to the thermal influence of the water column during lake inundation (Wellman *et al.*, 2013). Vegetation in the dried lake margin has progressed through ecological succession of open meadow to patchy colonisation by woody shrubs. Previous soil investigations (e.g. Jepsen *et al.*, 2012), combined with field analysis of soil pits and auger holes in this study, indicate that the shallow sediments in the mixed meadow are predominantly a silt loam underlain by gravel.

Toward the northwest corner of the lake, an oblong offshoot of the previously inundated zone now contains discrete patches of shrubs (predominantly willow), and more contiguous shrub bands that presumably reflect willow dispersal at intermediate lake levels (Figure 1). Shrub growth shades soil and intercepts infiltrating water in the summer, generating subtle variations in boundary conditions that differ from ambient grassy meadow conditions that permit the development of new, shallow permafrost (Briggs *et al.*, 2014). Therefore, within the dried lake margin and adjacent forest, a complicated mosaic of frozen and thawed soil existed in late summer of 2011 and 2012, when most data were collected for this study.

METHODS

Multiple surface geophysical methods were paired with physical data collection in a transitional landscape of discontinuous permafrost to investigate individual method sensitivity to subtle active-layer features and other transient permafrost features.

Physical and Thermal Methods

Direct observations made with push probes, soil augers and soil pits were used to augment surface geophysical data within the dried lake margin and adjacent forest. In late summer 2011 and 2012, a 3.7 m long metal rod (frost probe) was vertically inserted into the ground at approximately 1–5 m lateral intervals along line 2 from the forest (0 m) into the mixed meadow (100 m) (Figure 1) to determine if frozen ground was present; more widely spaced roving frost probe surveys were conducted throughout the meadow. In 2012, the frost probe tip was affixed with a digital thermometer (Traceable, Inc., Friendswood, TX, USA) to help distinguish refusal resulting from frozen ground from refusal by

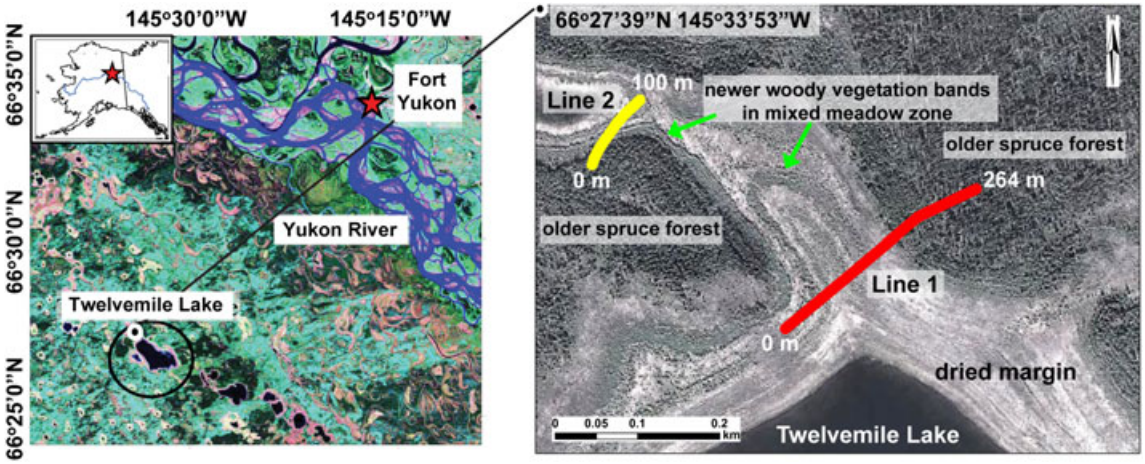

Figure 1 Location of the study area. Data collection was focused within the dried lake margin and adjacent boreal forests toward the northeast corner of Twelvemile Lake. The older spruce forest is underlain by thick, long-established permafrost, while past lake extents have caused complete thawing of old permafrost within the perimeter of the lake highstand, delineated by the forest border. Several decades of recent lake recession and vegetation succession, including woody shrub development, have promoted aggradation of discontinuous patches of permafrost in the dried lake margin. Repeated data collection with multiple methods was concentrated along lines 1 and 2, while broader surveys were conducted in the adjacent meadow and wooded areas. This figure is available in colour online at wileyonlinelibrary.com/journal/ppp

unfrozen gravel. An agricultural-grade soil moisture/temperature probe (EC-350, manufacturer-reported accuracy ± 1.5%, not field calibrated, Aquaterr Instruments & Automation, Inc., Costa Mesa, CA, USA) was used to point-sample the area at 0.75 m depth. In 2011, soil auguring was performed at select locations. Soil pits were manually excavated to ~ 2.2 m depth to directly investigate frozen soil distribution in areas of specific interest along lines 1 and 2. Detailed soil temperature and moisture profiles were collected along the sides of the pits using the digital thermometer, soil moisture probe and an infrared camera (FLIR T640bx, FLIR Systems, Inc.) (Figure 2).

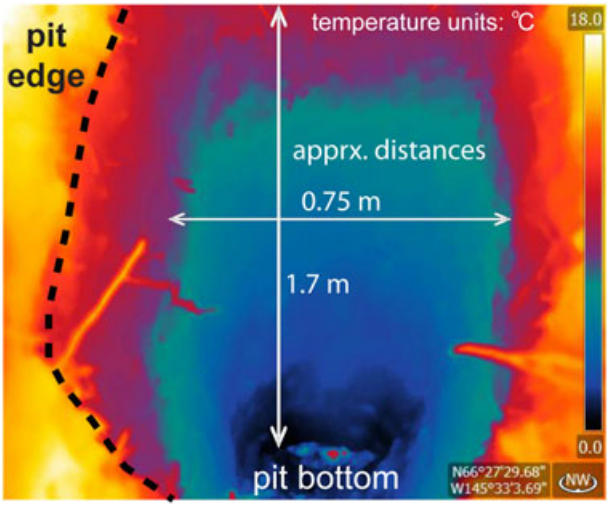

Figure 2 An infrared image (collected in August 2014) looking from above into a soil pit extending through the active layer to the top of the permafrost in the mature spruce forest; warm-coloured clumps of sediment at the pit bottom have fallen in from the surface. This figure is available in colour online at wileyonlinelibrary.com/journal/ppp

Electrical Resistivity Imaging

Direct current electrical resistivity imaging (ERI) surveys were collected at Twelvemile Lake in August 2012 using a Syscal Pro 10 channel instrument and a 48 electrode array (Iris, Orleans, France). The steel electrodes were installed into the shallow subsurface at 2 m spacing laterally along line 2 (Figure 3a); a second survey with 0.5 m electrode spacing was collected along a subset of line 2 from 70.5 to 94 m (Figure 3c). Roll-along arrays overlapped by 18 electrodes; the measurement sequence used a mix of 895-nested Wenner-array quadripoles designed to maximise the signal-to-noise ratio and the sensitivity to horizontal interfaces. Reciprocal measurements were collected by swapping the voltage and current electrodes to obtain an estimate of quadripole measurement error. Reciprocal measurement errors were used to assess data 'worth' and weight the data misfit in the resistivity inversion. Measurements with reciprocal errors greater than 2 per cent were removed, as were data with unreasonable values such as zero injection current; application of these criteria eliminated 28 out of 895 measurements.

The two-dimensional (2D) image of subsurface resistivity distribution was estimated by solving a regularised optimisation inversion problem where the data misfit plus a smoothing parameter is minimised. The inversion was carried out using the R2 code (Binley, 2015). The forward model was calculated using a quadrilateral mesh with a spacing one-quarter that of the electrode spacing. Model sensitivity estimation was used to determine the appropriateness of the model and assess the ERI survey depth of investigation.

Multi-Frequency EMI

A hand-carried EMI instrument (GEM-2, manufactured by Geophex, Inc., Raleigh, NC, USA) was used in

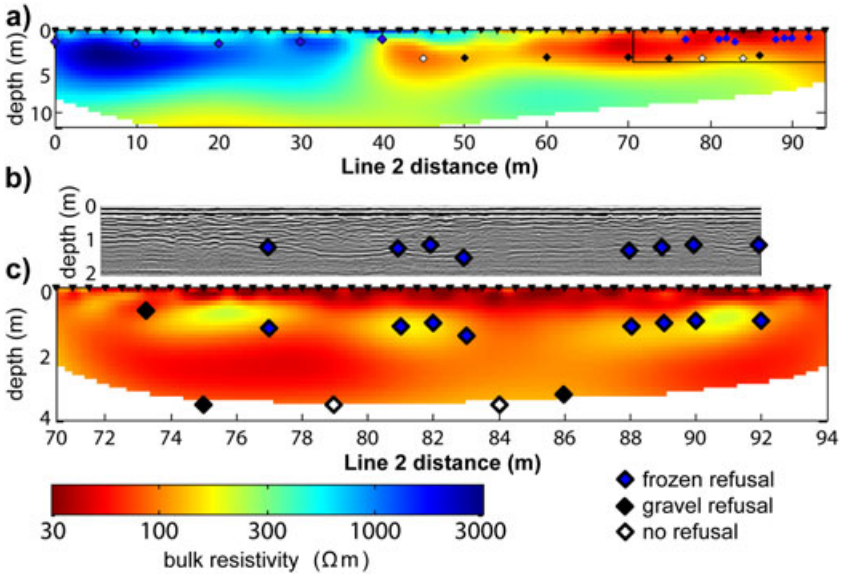

Figure 3 Line 2 data from combined methods: (a) inversion of 2012 electrical resistivity imaging (ERI) data with 2 m electrode spacing and related frost probe data; (b) 2011 GPR data from a subset of line 2 within the box indicated in (a); and (c) 2012 ERI data with 0.5 m electrode spacing from a subset of line 2 within the box indicated in (a). The larger electrode spacing shows the zone of thick, old permafrost, deep gravel lens and predominantly thawed meadow area but the new permafrost is not well captured. The closer electrode spacing along a subset of the line does capture the shallow, thin frozen features that correspond with frost probe data. Although collected a year prior, the GPR data show a discontinuous reflector that corresponds with frost probe and 0.5 m ERI data.

2011 and 2012 to measure the subsurface electrical conductivity of thawed and frozen ground in the northeast corner area of Twelvemile Lake. Multi-frequency (n = 7) quadrature data ranging from 1530 to 93 kHz were used to estimate subsurface electrical conductivity from approximately 0 to 12 m depth. The 2011 data were collected in vertical dipole mode to maximise penetration depth over a range of soil conditions, while the 2012 data were primarily collected in horizontal dipole mode to maximise sensitivity to the shallow permafrost and active-layer features.

The calibration and inversion of frequency-domain EMI data to accurately model subsurface conductivity can be challenging. To address this, the US Geological Survey (USGS) Branch of Geophysics and Rutgers University are developing codes for the inversion of frequency-domain electromagnetic data. This new code is an extension of an EMI code previously described by Schultz and Ruppel (2005) with additional features and capabilities, including one-dimensional (1D) laterally constrained electromagnetic inversion, and regularisation and inversion in 2D or three dimensions (3D; user defined), although the forward models are in 1D, in order to minimise problems commonly associated with other unconstrained 1D approaches (e.g. Auken *et al.*, 2006; Minsley *et al.*, 2012b). A parallel inversion capability greatly speeds the processing of large data-sets such as that collected at Twelvemile Lake. Prior to inversion, we filter and calibrate the data following the approach suggested by Minsley *et al.* (2012b). With this approach, the EMI data are adjusted against a conductivity model derived from ERI surveys. Regularisation is implemented using the Tikhonov (1953) approach.

GPR

GPR profiles were collected at Twelvemile Lake during the 2011 and 2012 summer field campaigns. A GSSI SIR-3000 control unit (Geophysical Survey Systems, Inc., Nashua, NH, USA) coupled with a GSSI model 5103 400 MHz centre-frequency bistatic antenna was used to assess: (1) the near-surface lithological properties; (2) the presence of frozen ground; and (3) the depth and spatial extent of the active layer. The antenna was hand towed at approximately 0.5 m s^{-1} across transects (e.g. lines 1 and 2) mostly cleared of surface vegetation to improve antenna coupling and subsurface signal penetration. The antenna was oriented orthogonal to the profile direction. The recording time window ranged from 80–140 ns with 1024–2048 16 bit samples recorded per trace. Profiles were recorded using time–range gain, band pass filtering and stacking to reduce noise and improve reflector signal-to-noise ratios. Distance marks every 10 m were used to distance-normalise (rubber-sheet) each radar profile. All described GPR profile time ranges are two-way travel times (TWTT) unless otherwise noted.

Following distance normalisation, post-stack variable velocity migration was performed to convert reflection time to depth using RADAN (GSSI proprietary software) through reflection hyperbola matching to estimate the spatial distribution of relative permittivity (ε') and associated electromagnetic wave velocities. The location of each 10 m mark was also recorded with a handheld Garmin GPSMap62stc (Canton of Schaffhausen, Switzerland) and surface elevation corrections were applied to each radar profile using previously collected high vertical resolution airborne light detection and ranging (lidar) data.

GPR waveform polarity (phase) interpretations of reflection triplet sequences were performed as suggested by Arcone *et al*. (1995). That is, for the model antenna used, the polarity of the first three half-cycle responses of a reflecting horizon or target indicates the contrast in the ε′ between layers. The differences in ε′ of liquid water (~80), permafrost (~5.3), ice (~3.2), air (1) and sediments (~5–26 depending on moisture content) provide sufficient contrast to interpret triplet sequences in terms of differences in dielectric properties at reflector boundaries. A positive (+ - +) triplet suggests that the deeper layer or target has a higher ε′ than the overlying layer (i.e. more water or unfrozen), and a negative (- + -) triplet suggests that the deeper layer or target has a lower ε′ (i.e. less water or frozen).

Forward Modelling of Electrical Resistivity

To demonstrate the utility of the direct current ERI method to describe fine-scale permafrost features, synthetic resistivity models were developed based on typical silt loam soil conditions expected within the Twelvemile Lake dried margin (Jepsen *et al*., 2012). Seasonal frozen ground and permafrost dynamics were evaluated using the USGS SUTRA-ICE model that simulates coupled fluid flow and energy transport for variably saturated conditions with freeze/thaw (Mckenzie *et al*., 2007). The 1D SUTRA-ICE numerical simulations were designed to investigate the subsurface cryologic response to lake recession and vegetation succession in a cold region landscape (see Briggs *et al*., 2014, for a full description of the numerical analysis). SUTRA-ICE model output, including information on ice and liquid water saturation and temperature, was then converted to geoelectrical resistivity fields based on a version of Archie's (1942) law, a widely used petrophysical relation modified to enable consideration of liquid and solid water phases. This relationship assumes that soil bulk resistivity ρ (Ωm) is controlled by ionic conduction of the pore fluid in a two-phase medium:

$$\rho = \alpha \rho_w \theta^{-m} S_w^{-n} \quad (1)$$

For this work (and SUTRA-ICE modelling), a soil porosity (θ) of 0.46 for silt loam soils was assumed, based on laboratory measurements of similar soils (Watanabe *et al*., 2011). The fraction of pore space filled with liquid water (S_w) was obtained from the SUTRA-ICE model output; the ice is assumed to have no electrical conduction capability, similar to air-filled pore space. The empirically determined Archie's law parameters α, m and n were initially estimated as 1, 1.5 and 1.8, respectively (based on typical published values), and manually optimised to match a subset of collocated bulk resistivity, fluid conductivity and saturation field data acquired in 2012 at a depth of 0.75 m along line 1. The resistivity of the water ρ_w, 23.3 Ωm is from a 2012 field measurement of a water sample obtained from a test pit along line 1 using an Oakton handheld water conductivity meter (Oakton Instruments, Vernon Hills, IL, USA).

Soil resistivity was adjusted for temperature using the relationship:

$$\rho = \frac{\rho_o}{1 + \alpha_t (T - T_o)} \quad (2)$$

where α_t is the temperature coefficient 0.025 K^{-1} and $T\text{-}T_o$ is the change in temperature. In this study, other temperature-dependent effects on the resistivity of soil (including temperature effects below the freezing point and ion exclusion) were not considered, because the conditions modelled by SUTRA-ICE were typically close to the freezing point and ice saturation did not exceed 0.6 due to the relatively large percentage of liquid water (16.6%) expected in silt loams at temperatures as low as -20 °C (Watanabe *et al*., 2011). Resistivity was determined using Equations 1 and 2 for numerical model output for the lake recession scenario with willow shrub influence that promotes permafrost aggradation ('willow' model) and open meadow conditions within the dried lake boundary before ecological succession ('ambient' model); model output is at 10 d increments over 1 yr.

Quantitative evaluation of ERI resolution and depth of investigation based on modelling exercises for hypothetical, yet realistic field scenarios can guide planning of ERI surveys and support interpretation of ERI results. Here, we evaluate ERI resolution and depth of investigation as a function of electrode spacing, for scenarios based on the SUTRA-ICE model output and Equations 1 and 2. We use the R2 code forward resistivity model to simulate hypothetical ERI data for snapshots in late August (corresponding with fieldwork timing) for 0.5, 1.0, 2 and 4 m electrode spacing surveys. The willow model has several metres of new, shallow permafrost in late summer, whereas the ambient model has only a maximum ice saturation of about 5 per cent at the capillary fringe of the 3 m deep water table during the same time frame. The willow condition was applied to the left half of the domain and the ambient condition was applied to the right half, representing mixed meadow conditions of discrete woody vegetation clumps and shrub bands (willow condition) within the grassy area (ambient condition). The total domain width/depth varied based on electrode spacing and a constant number of virtual electrodes (n = 48); therefore for larger electrode spacing, the synthetic domain was both wider and deeper. To replicate typical field data errors, 2 per cent random noise was applied to the synthetic measurements and a resistivity field was estimated for each of the four variable spacing models using the same inversion method as the field case.

RESULTS

Data pertaining to shallow frozen ground distribution from physical, thermal, radar and electrical methods are presented below. ERI forward resistivity modelling based on SUTRA-ICE model output is used to guide field data interpretation

and survey designs for future applications by examining the geophysical response to 'known' conditions.

Physical Methods

Frost probe measurements along line 2 in 2012 indicated that the ALT averaged 1.5 m in the forest above thick, old permafrost (Table 1). For approximately 25 m from the wood's edge into the meadow, no frozen ground was observed via manual probing. Here, refusal at an average depth of 3.4 m indicated the top of a gravel layer. Frost probing from approximately 77 to 92 m along line 2 showed patchy frozen ground at an average depth of 1.14 m, where present, associated with shrub growth (Figure 3); this was interpreted as new permafrost aggradation. Temperature measurements at 0.75 m depth were consistently $< 3\,^{\circ}C$ above the new permafrost but warmer elsewhere; in contrast, 0.75 m depth temperature measurements were not a good predictor of older permafrost in the forest, where the active layer was thicker as temperatures at 0.75 m depth were similar to those of unfrozen profiles. Moisture measurements at 0.75 m depth were generally greater in the mixed meadow than in the forest, including many values near 90 per cent saturation due to recent heavy rains near the time of measurement.

A soil pit dug along line 2 in 2012 at 90 m revealed a discrete block of frozen ground at 1.15 m depth at least 1 m across; a thickness measurement was not possible. A similar but deeper pit at 0 m along line 1 in 2012 found low ice content and near-freezing temperatures at the water table at approximately 2.1 m, but unlike the contiguous frozen block of soil found in the pit of line 2, this relatively stiff soil could be penetrated. This pit contrasted with 2011 frost probing and soil pits from the same area of line 1, which indicated thicker zones of frozen ground with higher ice content. A larger 2012 survey of frost probing in locations of interest throughout the western side of the mixed meadow area showed a pattern of shallow frozen ground and cold temperatures (e.g. $< 3\,^{\circ}C$) at 0.75 m depth associated with willow vegetation.

ERI

The 2012 ERI surveys along line 2 exemplify how electrode spacing strongly controls shallow data resolution and depth of investigation (Figure 3). The survey with 2 m spacing from 0 to 94 m shows a strongly resistive zone below the forest from 0 to 38 m that corresponds with the expected signature (10^3–10^4 Ω m) for frozen silt in the area (e.g. Hoekstra, 1975) (Figure 3a). A less resistive shallow active layer is evident in the ERI data over the frozen silt; the interpreted depth of thaw matches the depth measured by frost probing along this forested segment. There is a transition to overall much more conductive material in the mixed meadow area (40 to 94 m along line 2, Figure 3), particularly to a depth of approximately 4 m. Below 4 m, a resistive (200–600 Ω m) zone likely represents saturated gravel expected in the area (Froese *et al.*, 2005), and the interpreted 4 m deep lithologic transition to gravel corresponds with frost probe data (Figure 3a, c; Table 1). The shallow horizon

Table 1 Frost probe data and temperature and moisture measurements at 0.75 m depth along line 2 collected in 2012.

Line 2 distance (m)	Depth frozen refusal (m)	Depth gravel refusal (m)	Temperature at 0.75 m depth (°C)	Moisture at 0.75 m depth (% sat)
0	1.44	-	3.9	62.4
10	1.64	-	3.2	46.4
20	1.63	-	4.0	68.5
30	1.47	-	3.6	84.2
40	1.28	-	4.5	59.0
45	-	3.70+	4.1	52.7
50	-	3.40	4.8	69.2
60	-	3.38	4.4	70.7
70	-	3.38	6.6	90.8
75	-	3.53	4.4	90.1
77	1.21	-	2.2	92.1
79	-	3.70+	3.6	90.5
81	1.18	-	2.0	92.3
82	1.04	-	2.2	89.1
83	1.44	-	2.9	91.4
86	-	3.18	3.6	84.2
88	1.17	-	1.8	88.6
89	1.06	-	1.6	89.2
90	1.03	-	1.8	n/a
92	0.99	-	2.0	88.9
95	-	3.70+	n/a	n/a
100	-	3.70+	6.6	94.4

Darker shading indicates wooded locations with thick, older permafrost; light shading indicates locations where new permafrost associated with shrub growth was found. n/a = Not available.

(<4 m depth) in the meadow is an order of magnitude less resistive, reflecting predominantly unfrozen silt loam with high moisture content (Table 1). Local permafrost aggradation identified with frost probing is not captured well by the 2 m electrode spacing, although there are some indications of subtle variation in resistivity in the new permafrost area (Figure 3a inset box).

The ERI survey using 0.5 m electrode spacing from 70 to 94 m shows shallow resistive lenses (200–400 Ω m) that correspond with frost probe data, indicating permafrost aggradation since the retreat of the lake (Figure 3b). Lateral breaks in the resistive lenses also correspond to places were thawed ground was identified via probing. The ERI data indicate that the newly aggraded permafrost is approximately 1 m thick and exists wholly within the upper 2 m. Although ERI data resolution has seemingly been greatly improved with the closer electrode spacing, the depth of investigation is limited to approximately 3 m. Data from both electrode spacings were used to calibrate EMI data to the study area field conditions.

Multi-Frequency EMI

EMI data collected with the GEM-2 instrument in 2011 and 2012 were calibrated and inverted, yielding a spatially distributed model of shallow subsurface conductivity across the mixed meadow areas (Figure 4). Zones of lowest conductivity at 1 m depth in the 2011 vertical dipole mode model generally coincide with the spruce forest, but also to topographic highs. A 'nearest-neighbor' interpolation of the data performed in ArcMap 10.0 (Esri, Inc., Redlands, CA, USA) shows apparent gradients in bulk conductivity that track the topography, with higher conductivity zones in low-lying areas toward the lake (Figure 5).

The 2012 EMI survey performed in horizontal dipole mode (which maximises shallow subsurface resolution) in the meadow area of permafrost aggradation reveals more subtle resistive features at 1 m depth (Figure 4). Throughout the mixed meadow area are intermingled zones of varied conductivity, some of which show spatial continuity when the measured data are interpolated in 2D (Figure 5). The interpolated data show a large swathe of less conductive ground coinciding with banded willow growth, indicating that this vegetation is underlain by more contiguous newly formed permafrost than observed under the patchy vegetation of line 2 (Figure 5). This interpretation is supported by frost probing throughout the meadow area (Figure 6). A closer look at a particularly large willow patch underlain by new permafrost and an area of banded vegetation at varied depths (0.5, 1.0, 2.0 m) shows that the resistive zones associated with permafrost aggradation are visible at all these shallow depths, although they are greatly diminished by 2.0 m (Figure 6). These data agree with the ERI survey, which indicated that new permafrost was approximately 1 m thick (Figure 3). Several of the more open meadow areas are considerably more conductive at 2.0 m depth, potentially indicating higher moisture content (Figure 6c), which would coincide well with the nearby line 1 soil pit that reached the water table at 2.1 m depth.

GPR

Maximum depth of penetration for the 400 MHz GPR antenna in the study area was approximately 3 m. Regions with shallower penetration depths are interpreted as low-resistivity thaw zones with high free-water content or silt fraction. Maximum penetration occurred within the higher-elevation forested areas where shallow permafrost, which is highly resistive, is overlain by drier thawed silts. Relative permittivity (ε') calculated from ground truth provided by frost probing permafrost reflectors ranges from a value of 5 in drier areas to 26 in wetter areas, consistent with ranges

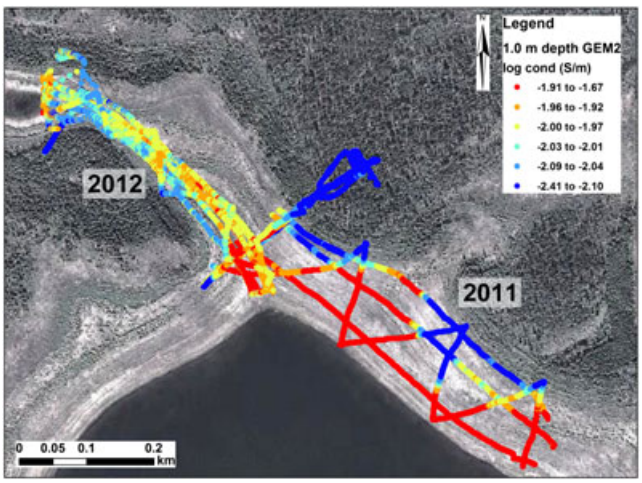

Figure 4 A map view of the calibrated 1.0 m depth GEM2 data from both the 2011 (right) and 2012 (left) surveys within the dried lake boundary and adjacent spruce forest. Systematic changes in ground conductivity are observed in adjacent lines, with the most conductive areas located in low open areas near the lake (with likely higher moisture content) and the least conductive zones generally within the spruce forest over thick, old permafrost. This figure is available in colour online at wileyonlinelibrary.com/journal/ppp

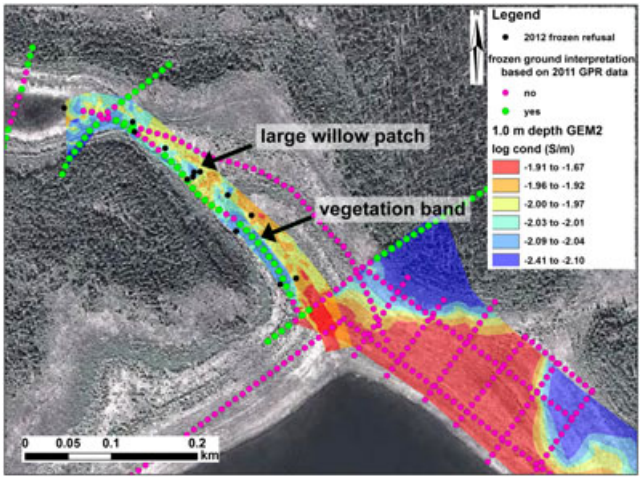

Figure 5 A two-dimensional interpolation of the 1.0 m depth GEM2 data shown in Figure 4 combined with interpretations of frozen ground at any depth indicated by 2011 GPR profiles. The 2012 data collected in the mixed meadow area show a relation between the 'bathtub rings' of thicker willow and less conductive zones along with GPR-indicated frozen ground. Black dots indicate where frost probing on the edge of willow patches identified newly formed permafrost. This figure is available in colour online at wileyonlinelibrary.com/journal/ppp

reported in similar studies (Lawson *et al*., 1996; Arcone *et al*., 1998). The radar profiles from the northwest lake margin reveal shallow (0–2 m depth), dipping and discontinuous reflectors interpreted as sand, silt and clay layers that prograded as a result of migration and infill of the lake outflow channel. Sub-horizontal and relatively continuous reflectors within GPR profiles are interpreted as either the water table, older permafrost, or discontinuous new permafrost; specific reflector interpretation depends on the GPR triplet phase change at each horizon (Arcone *et al*., 1995). In general, GPR-based profile classification of permafrost in 2011 agrees with the EMI data from both 2011 and 2012 (Figure 5).

GPR data were collected along lines 1 and 2 during the 2011 and 2012 summer field campaigns. Because the 2012 data appear to be affected by high near-surface soil moisture content, the 2011 data are primarily shown here. Most profiles show shallow, short, dipping discontinuous reflections interpreted as sedimentary lenses of intermixed sands and silts (e.g. $<$ 1 m depths, Figures 3 and 7). Line 2 data from 2012 show a sub-horizontal reflective horizon at 25–42 ns (~1 m depth) that correlates with highly resistive discontinuous lenses observed in the 2012 ERI model in the mixed meadow area (Figure 3c). The reflective horizon, interpreted as the top boundary of permafrost, is more continuous in the 2011 GPR data than is indicated by the 2012 ERI survey and frost probing data; this finding is consistent with the interpretation from line 1 data that more frozen ground existed in late summer in the meadow area in 2011.

A direct comparison of a subset of line 1 GPR data between 2011 and 2012 indicates a more contiguous, strong reflector in 2011. The first 50 m of this profile is in open willow thickets mixed with high grassland and reveals a continuous horizon in 2011 from 0–50 m at 25–30 ns TWTT (~0.8–1.4 m depth). The triplet sequence suggests a transition from higher ε' above the horizon to lower ε' at the horizon. This horizon was interpreted as a transition through a thin (~20–50 cm thick) frozen layer. This interpretation is supported by frost probe data every 10 m and an auger hole drilled at a distance of 11 m on line 1. The same profile collected in 2012 revealed a weaker, less continuous and deeper horizon with the same triplet sequence from 0 to 40 m. As noted above, 2012 GPR data may have been adversely affected by elevated shallow moisture content due to recent precipitation, which could obscure frozen features. However, frost probe and soil pit data confirm the interpretation of a greater spatial distribution of frozen ground in this open area in 2011.

Large-scale roving GPR surveys in 2011 and 2012 were interpreted every 10 m for indicators of frozen ground to develop a simplified binary classification map (Figure 5). A regular grid survey in 2011 did not indicate any frozen ground in the area southeast of line 1, but did indicate frozen ground along the beginning of line 1 and the farther forested stretch of line 1. Similarly, a profile along line 2 and across a depression to the west of line 2 indicates discontinuous frozen ground that is most contiguous in the forested areas. Two GPR profiles were collected in August 2012 through the mixed meadow area between lines 1 and 2 (Figure 5). A lidar-based 2.5 m resolution digital elevation model shows that the southernmost profile though the meadow area has a northeast-facing slope aspect, whereas the northernmost profile though the meadow area has a southwest-facing slope aspect. Likewise, a slight vegetation shift from pockets/bands of willow and grasses to mostly grass occurs from the southern to northern profiles, respectively. The southern profile shows a shallow and nearly continuous frozen layer as a horizon at ~ 30 ns (approximately 1.5 m depth) along its entire length, whereas the northern profile shows no such horizon. Frost probing confirmed

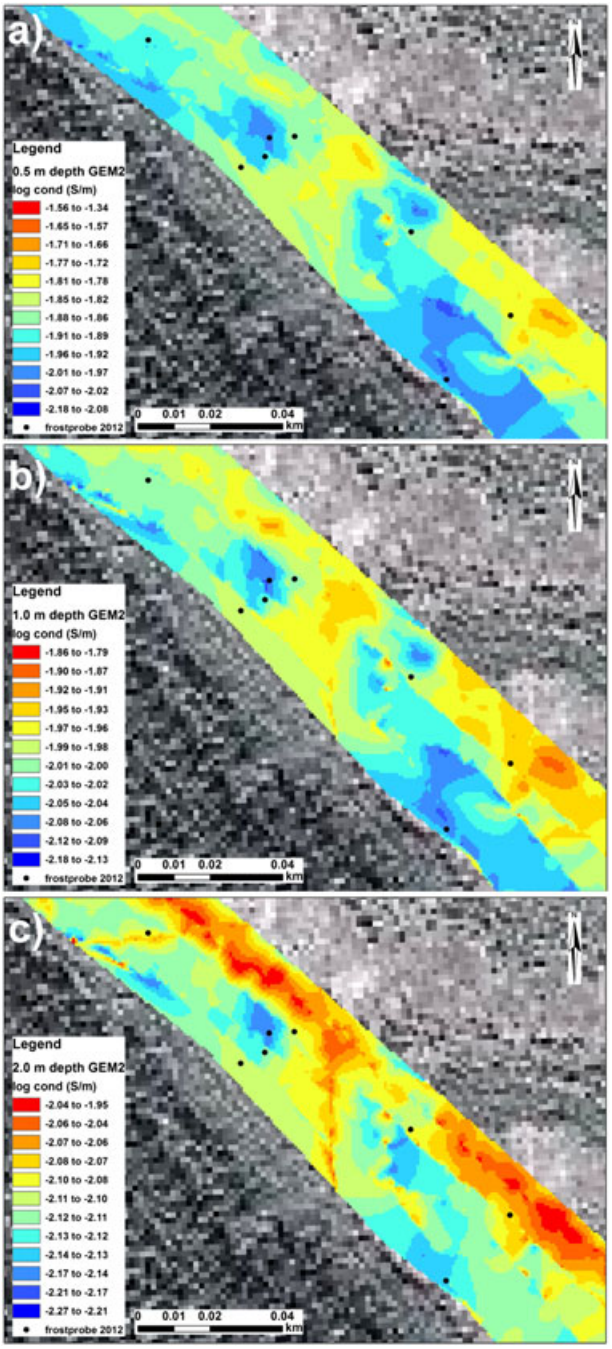

Figure 6 A close up of 2012 GEM2 data interpolations from the willow field area. Consistent less conductive zones are shown in both the (a) 0.5 m depth and (b) 1.0 m depth data, while some features are lost by the (c) 2.0 m depth. Less conductive zones correspond with known areas of willow vegetation and new permafrost that are roughly defined by frost probe measurements. As a result of decreasing total range and mean conductivity with depth, each plot is shown using independent colour scales. This figure is available in colour online at wileyonlinelibrary.com/journal/ppp

the existence of a shallow frozen layer along line 1, and temperature measurements at ~ 1 m depth confirmed lower ground temperatures relative to line 2. Substantial ringing below the interpreted frozen horizon is assumed to represent multiples caused by internal reflections between the frozen layer and saturated silt-rich sediments below, indicating that the frozen layer is relatively thin.

Resistivity and Forward Modelling

The transient SUTRA-ICE model results for the willow model over 1 yr of active-layer development above newly aggrading permafrost show strong seasonal variability with respect to temperature (Figure 8a, e), liquid water saturation (Figure 8b, f) and ice saturation (Figure 8c, g), as expected. For comparison, the ambient model output is shown for each parameter (Figure 8a–d) at the same late summer time simulated in Figure 9. The predicted resistivity profiles, created using Equations 1 and 2 at each time step, indicate that delineation of the active layer will be most evident using surface ERI methods in late winter and late summer because the largest resistivity contrast between the active layer and the shallow permafrost below occurs during these seasons. The time of maximum depth of annual soil thaw (i.e. ALT), as predicted by the SUTRA-ICE model, coincides with the time just following the Twelvemile field trips in early fall; observation of this more conductive zone is complicated by predicted near-surface drying in this area that increases resistivity. Relatively high ice saturation combined with low liquid water saturation and low temperatures makes the active layer more resistive than the underlying permafrost in late winter. The transition periods of late spring and late fall provide the least contrast between the active layer and permafrost.

Resistivity models derived from numerical SUTRA-ICE model output describing new permafrost formation under willow shrubs and seasonal freeze/thaw dynamics in the adjacent ambient meadow (Figure 9a) were used to create forward-modelled ERI inversions (Figure 9b–e); these examples indicate which frozen soil features may be practically resolved through application of the ERI method under different electrode configuration. As expected, there is a strong control of electrode spacing on near-surface data resolution and depth of investigation. Along the willow side of the 0.5 m electrode spacing inversion (Figure 9b), the more conductive horizon separating the dry near-surface and the new permafrost is strongly smeared out. The ambient side of the model domain (no permafrost) shows a resistive zone in the upper metre due to the dry near-surface conditions expected in late summer. The shallow depth of investigation of approximately 4 m does not reach to the bottom of the simulated permafrost, and so thickness is not well constrained. The 1 m electrode spacing was similar, although the bottom of the new permafrost is better suggested by the inversion (Figure 9c). The 2 m electrode spacing perhaps best captures both the ALT above the permafrost lens and the approximate thickness of frozen ground (Figure 9d); the active-layer subtleties are lost with the 4 m spacing, but the estimated thickness of permafrost is similar to the inversion with 2 m spacing applied (Figure 9e).

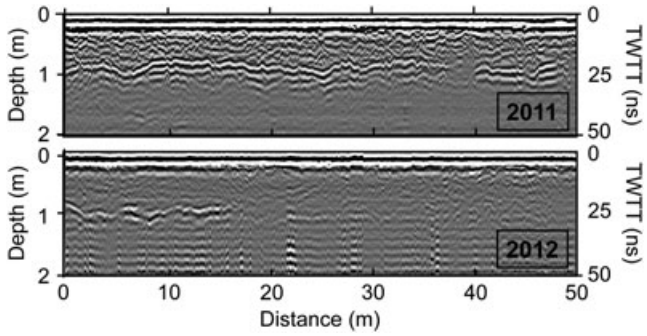

Figure 7 GPR profiles from 0 to 50 m along line 1 in 2011 and 2012. The stronger reflective horizon observed in 2011 indicates a more contiguous and higher ice-content frozen layer at approximately 1 m depth compared to that in 2012; this interpretation was supported by physical measurements. TWTT = Two-way travel time.

The low ice content (approximately 5%) zone that develops in the ambient meadow models near the capillary fringe is not resolved in any inversion.

DISCUSSION

The complex permafrost distribution around Twelvemile Lake allowed the direct comparison, augmented by forward resistivity modelling, of several geophysical techniques in evaluating shallow frozen ground dynamics. ERI methods provided the most robust 2D images of permafrost along designated transects, but EMI and GPR methods enabled efficient coverage of large areas and also revealed important active-layer and permafrost features. The existence of transient frozen ground was evident by comparison between the 2011 and 2012 surveys in EMI and GPR data, interpretations that are supported by physical measurements, indicating the ability of these methods to delineate thin, transient and discontinuous frozen ground features.

Evaluating Shallow Frozen Features

The upper boundary of the thick (up to approximately 90 m) permafrost expected below the mature forests outside of the historical lake highstand boundary (Minsley *et al.*, 2012a) is observed with all three geophysical methods in both 2011 and 2012. The 2012 ERI data (2 m electrode spacing)

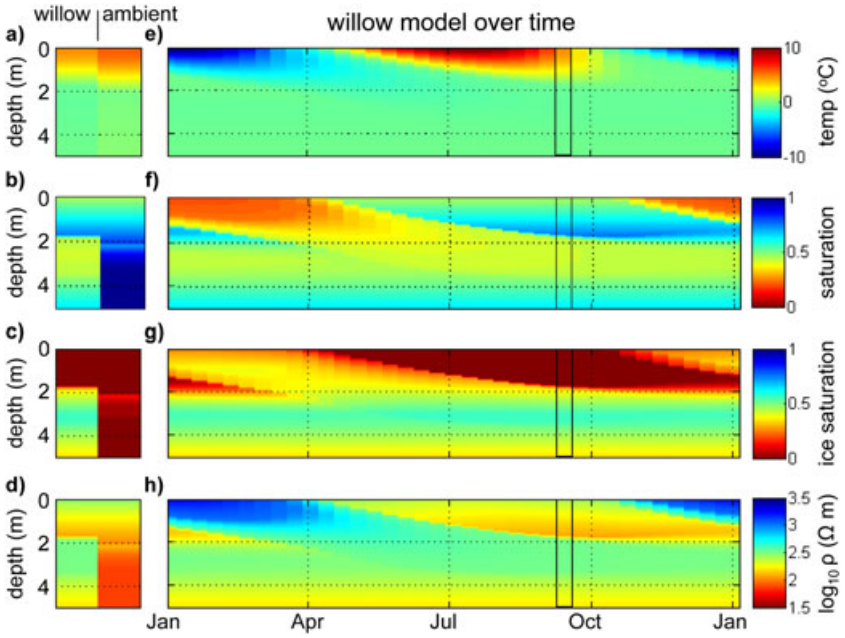

Figure 8 Distributions by depth for simulated late summer in Figure 7 are shown for the willow and ambient models for the parameters: (a) temperature; (b) liquid saturation; and (c) ice saturation; these parameters drive subsurface resistivity shown in panel (d). Temporal distributions of these parameters are shown for the willow model in panels (e)–(g) at 10 d intervals, and are used to calculate the expected resistivity profile time series shown in (h). The open box corresponds to the timing of model output shown in (a)–(d). This figure is available in colour online at wileyonlinelibrary.com/journal/ppp

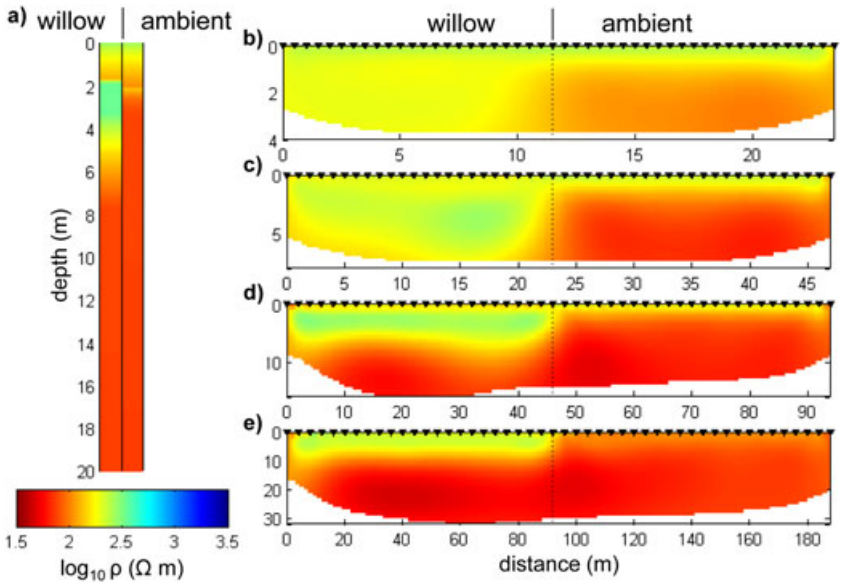

Figure 9 Panel (a) SUTRA-ICE simulations of the ambient (no permafrost) meadow condition and willow condition (i.e. thin (approximately 3 m) newly formed permafrost under willow growth) were used to derive expected resistivity profiles. From this known resistivity, inversions were developed for a willow-ambient spatial transition based on simulated electrode spacing, ranging from: (b) 0.5 m; (c) 1 m; (d) 2 m; and (e) 4 m. Size of the inversion domains is controlled by electrode spacing, with larger intervals enhancing the depth of investigation but reducing data spatial resolution. This figure is available in colour online at wileyonlinelibrary.com/journal/ppp

collected along line 2 show a strong resistive zone, the end of which coincides with the forested transition to mixed meadow in the dried lake margin (Figures 1 and 3). Delineation of the active layer above this thick permafrost is subtle but resolvable in the ERI data, and compares reasonably well with frost probe data. It is likely that recent rains and subsequent high soil moisture (46–84% saturation) increase 'visibility' of this upper layer by providing greater electrical contrast with the resistive frozen zone than would typically be expected from the typically drier woodland silts (Jepsen *et al.*, 2012). GPR data collected here and along the forested sections of line 1 also indicate the presence of permafrost, with a more precisely defined active-layer boundary than ERI is able to resolve. However with GPR, the conversion from measured velocity to reflector depth is controlled by ε', which is highly variable in space along line 2 ($14 \leq \varepsilon' \leq 26$), and so depth controls provided by physical frost probing are useful for calibrating GPR interpretations. The EMI results also consistently show resistive permafrost in heavily forested areas; with EMI, active-layer detail is affected by the mode of data collection (horizontal or vertical dipole), as discussed below.

Discontinuous, and likely recently formed, permafrost is indicated along line 2 by physical frost probe and temperature measurements. Ground temperatures collected at a common depth (0.75 m) are shown to be useful in indicating permafrost aggradation on this transect. Along line 2, temperatures $< 3.0\,^{\circ}\mathrm{C}$ always coincide with the shallower discontinuous permafrost. Because conduction of heat is gradient-driven diffusion, a linear gradient is expected between permafrost and the ground surface in the absence of rapidly changing surface temperatures (thus yielding disequilibrium conditions) or substantial infiltration of water (thus inducing advective heat flow). Therefore, synoptic temperature evaluations at specific depth may be useful for developing site-specific empirical relations to estimate ALT. Infrared data collected at extremely high (e.g. millimetres) spatial resolution along the newly exposed walls of active-layer soil pits may provide data useful in numerical model calibration at a scale not before possible (Figure 2). Preferential flow process can also be indicated by high-resolution thermal patterns, assuming that infiltration water is in disequilibrium with the bulk soil matrix, though evidence of this phenomenon was not observed here.

ERI data (2 m spacing) from the mixed meadow area capture the transition from wet silt loam to gravel at approximately the 4 m depth (Figure 3a), but the recently formed, thin frozen features are not evident at this larger electrode spacing. However, tighter 0.5 m spacing greatly improves shallow data resolution and the discontinuous resistive frozen features favourably match the physical data (Figure 3c). These ERI data provide a thickness estimate for the new permafrost (approximately 1 m), which was not possible with surface probing and soil pits alone. GPR data from the same line 2 segment in 2012 indicate similar features, although a thickness estimate was also not possible (Figure 3b). Further, the near-surface wet conditions (approximately 90% saturation) that enhanced ERI contrasts between unfrozen and frozen soil in 2012 likely decrease the effectiveness of GPR by damping the signal. This contrast between methods shows that recent antecedent conditions must be taken into account when collecting and interpreting near-surface geophysical data to indicate permafrost features. As EMI data were calibrated to ERI data along line 2 data, they are not compared directly along this line.

Interestingly, the forward resistivity modelling of permafrost aggradation indicates that the active layer would not be well captured by ERI at any electrode spacing but that the general thickness of frozen soil would be captured by a 2 m spacing, in direct contrast to results from the field data. This apparent discrepancy can be explained by the unusually high soil moisture field conditions in 2012, and the greater thickness (factor of 4x) of modelled permafrost compared to what was observed in the field. As mentioned above, soil moisture increases the contrast between the active layer and frozen ground (e.g. Figure 8 f, h). The SUTRA-ICE models were developed based on the average summer precipitation of 0.1 m (Snow Telemetry (SNOTEL) #961); therefore the simulated active layer is relatively dry and resistive (Figure 9) and harder to distinguish from frozen ground compared to observed field conditions in 2012. The model results used here represent the expected permafrost distribution near steady state after many decades of willow shrub persistence, and therefore the frozen features are thicker than observed, as the field site has been colonised by woody shrubs for < 25 yr. When a layered transition exists from a conductive active layer to resistive thin frozen ground, and back to conductive saturated and lower unfrozen ground, the frozen features can be smeared out with larger electrode spacing (e.g. 2 m field data) if the frozen soil is too thin. However, thicker frozen features may be better captured with ERI, and larger spacing permits deeper investigation and a quantification of the lower frozen boundary not possible with other surface methods.

Although ERI data provide useful insights regarding the distribution of frozen ground, application of the method over broad areas is limited by the time and effort required to transport and set up the equipment, and to acquire the field measurements. EMI and GPR coverage exceeded ERI coverage by more than an order of magnitude over similar duration investigations (days). Interpreted GPR data capture both the new permafrost in the mixed meadow and long-established permafrost in the forest (Figure 5). The rapid rate of GPR data collection relative to other geophysical methods (which require substantial set-up or take down time, involve large amounts of equipment, or require substantial processing) is valuable because the method can be used as a reconnaissance tool to determine ALT or the absence of permafrost, nearly in real time. However, experience and skill are required to robustly interpret GPR data, particularly for lower-quality data or when sedimentary features create additional reflectors, and where profiles are complicated by buried organic matter and cryoturbation features (Hinkel *et al*., 2001).

The 2011 EMI data, collected in vertical dipole mode, appear to primarily capture topography-driven moisture differences in areas dominated by meadow grasses and small shrubs; GPR data collected in the same area do not indicate frozen ground (Figure 5). The 2012 EMI survey collected using the higher shallow resolution horizontal dipole mode indicates a strong relation between new permafrost features and shrub growth in the meadow area (Figure 5). When the data are spatially interpolated, the resulting map shows that permafrost aggradation is more contiguous than suspected from line 2 data alone, particularly under thicker bands of shrub growth (Figures 5 and 6). Although the depth of investigation was limited to approximately 2 m, the multi-frequency data allow depth-specific measurements for pseudo-3D interpretation; therefore thickness of the shallow frozen features can be interpreted. Considerable post-processing is required of EMI data, but the ease of data collection exceeded that for GPR as vegetation did not need to be cleared, and the data were improved (instead of hindered) by the wet conditions. EMI also has potential value for integration with large-scale airborne electromagnetic data, capable of mapping permafrost distribution at landscape scales (Minsley *et al*., 2012b; Pastick *et al*., 2013).

Monitoring Temporal Changes

Disturbance, ecological feedback mechanisms and natural and human-impacted climate cycles may affect shallow permafrost distribution and ALT. There is a need to monitor changes in frozen ground through time using surface-based methods that balance efficient spatial coverage with the resolution required to image local and transient subsurface features. In this case study, soil pits and frost probing indicated patchy frozen soil along line 1 in 2011, but not in 2012; this finding suggests that frozen ground observed in August 2011 was the result of transient conditions favourable to permafrost. This multi-year comparison further suggests that conditions in the Twelvemile Lake meadow represent a tipping point for permafrost stability, and that controlling variables such as the thickness and onset of snowpack and the temperature and precipitation in summer may cause measureable year-to-year variability. These frozen features would not likely be classified as part of the transition zone as defined by Shur *et al*. (2005), as airborne EMI data indicated that they were not underlain by stable permafrost but instead existed within the open vertical talik that connects to the lower regional aquifer. Local transient frozen ground such as this is sometimes termed 'pereletok', and there has been some question regarding the efficacy of GPR to resolve such features (Hinkel *et al*., 2001). The 400 MHz antenna used for this study is apparently suitable for application to thin, transient frozen features of varied ice content. The 2011 GPR data from line 1 and line 2 (not shown) indicate new permafrost that was more contiguous than in 2012 (Figure 7), and therefore capture this interannual variability in shallow ground ice. EMI and ERI data collections could not be directly compared spatially between the 2 yr, but longer-term changes in the transition layer above thick permafrost are likely visible using all three geophysical methods

Forward modelling was used to evaluate the potential effectiveness of ERI (and EMI) in quantifying annual active-layer development using spatially consistent time-lapse monitoring (Figure 8). The resulting resistivity profiles strung together at 10 d intervals indicate that active-layer resistivity changes of approximately two times

can be expected when the effects of ion exclusion during freezing are neglected. The strongest contrasts between the active layer and permafrost occur in late summer (Figure 8h); hence the applicability of ERI for active-layer dynamics may be seasonally limited.

To fully understand the capabilities of ERI, it is not sufficient to solely consider resistivity contrast; rather, array design, survey layout and data measurement errors play important roles that contribute to overall model resolution and depth of investigation. Figure 9 shows inversion results for a site with a spatial transition between open grassy areas (ambient model) and woody shrub (willow model) conditions, representative of the observed mixed meadow. Inversion results indicate that the active layer is not well resolved when the active layer is relatively dry (Figure 9), regardless of the electrode spacing considered. This result indicates that during transitional times of the year shallow, thin features may be even more difficult to resolve, but that enhanced ground saturation after precipitation events can aid contrast between frozen and unfrozen soil. Interestingly, when the active layer freezes to maximum depth in mid-late winter, this layer is approximately 40 per cent more resistive than the permafrost below due to the additive effects of low temperature and low moisture content. With time-lapse ERI, analysis of difference maps often indicates processes not obvious in 'snapshot' data alone, and may be more useful in identifying changes in frozen ground features throughout the year and after disturbance.

CONCLUSIONS

The complicated distribution of frozen ground and permafrost around Twelvemile Lake in the Yukon Flats of interior Alaska provides an opportunity to integrate several surface geophysical methods (ERI, EMI, GPR, infrared) to evaluate ALT and longer-term transient frozen ground features, and highlight the methods' strengths and shortcomings. Data collected over several years indicated that thick, stable permafrost exists below mature forest adjacent to an area of mixed meadow within the dried lake boundary with newly aggraded permafrost and seasonally frozen ground. The active layer was thinner over the newly formed permafrost features, conditions that were confirmed with direct measurement of thaw depth and temperature.

Transferable lessons from this case study include:

1. ERI provided the best-constrained thickness estimates of thin, shallow permafrost features, followed by EMI.
2. Field data and forward resistivity modelling indicate that precise ALT estimates may not be possible with snapshot-in-time ERI and EMI surveys, though contrast is enhanced after rain events; GPR more clearly showed the upper interface of frozen ground, but the conversion to true depth is sensitive to the relative permittivity (ε') parameter, which may be highly spatially variable.
3. Practical spatial coverage was highest with EMI, followed by GPR; therefore, these two methods are most applicable to landscape-scale evaluations of transient frozen features relevant to research regarding shallow groundwater flow and surface water exchange.
4. GPR data can be evaluated in near-real time by an experienced practitioner, while EMI calibration and inversion involve more effort.
5. Infrared data collected along fresh soil pit walls in the active layer offer unprecedented detail of soil temperature data, and may be useful in the calibration of emerging variably saturated freeze-thaw numerical modelling techniques (e.g. SUTRA-ICE, Mckenzie *et al.*, 2007; ATS, Atchley *et al.*, 2015).

The distribution of shallow frozen ground in the discontinuous permafrost zone is vulnerable to change due to a combination of climate, disturbance and ecosystem-feedback effects. Indirect, geophysical methods are crucial tools to evaluate frozen soil dynamics over focused plot and landscape scales. As shown here, ERI, EMI and GPR have complementary but unique attributes; care must be taken when choosing a suite of methods for specific remote field campaigns. Time-lapse geophysical monitoring may provide additional insight into active-layer dynamics, as changes are commonly easier to detect in time-lapse than 'snapshot' surveys.

ACKNOWLEDGEMENTS

We thank Stephanie Saari, Emily Voytek, Heather Best, Doug Halm and Eric White for assistance in the field and in the processing of data. The manuscript was improved through journal review and by thorough feedback from Josh Koch. Funding for this project was provided by the Strategic Environmental Research and Development Program (award RC-2111), with additional support from the USGS Office of Groundwater, the USGS National Research Program and the USGS Groundwater Resources Program. Any use of trade, firm or product names is for descriptive purposes only and does not imply endorsement by the US Government.

REFERENCES

Archie GE. 1942. The electrical resistivity log as an aid in determining some reservoir characteristics. *Trans. AIME*, **146**: 54–62.

Arcone SA, Lawson DE, Delaney AJ. 1995. Short-pulse radar wavelet recovery and resolution of dielectric contrasts within englacial and basal ice of Matanuska Glacier, Alaska, U.S.A. *Journal of Glaciology* **41**: 68–86.

Arcone SA, Lawson DE, Delaney AJ, Strasser JC, Strasser JD. 1998. Ground-penetrating radar reflection profiling of groundwater and bedrock in an area of discontinuous permafrost. *Geophysics* **63**: 1573–1584.

Atchley AL, Painter SL, Harp DR, Coon ET, Wilson CJ, Liljedahl AK, Romanovsky VE. 2015. Using field observations to inform thermal hydrology models of permafrost dynamics with ATS

(v0.83). *Geoscientific Model Development* **8**: 2701–2722. DOI:10.5194/gmd-8-2701-2015

Auken E, Pellerin L, Christensen NB, Sørensen K. 2006. A survey of current trends in near-surface electrical and electromagnetic methods. *Geophysics* **71**: G249–G260. DOI:10.1190/1.2335575

Binley A. 2015. R2: Summary. Lancaster University.

Briggs MA, Walvoord MA, Mckenzie JM, Voss CI, Day-lewis FD, Lane JW. 2014. New permafrost is forming around shrinking Arctic lakes, but will it last? *Geophysical Research Letters* 1–8. DOI:10.1002/2014GL059251

Frampton A, Painter SL, Destouni G. 2012. Permafrost degradation and subsurface-flow changes caused by surface warming trends. *Hydrogeology Journal* **21**: 271–280. DOI:10.1007/s10040-012-0938-z

Froese DG, Smith DG, Clement DT. 2005. Characterizing large river history with shallow geophysics: Middle Yukon River, Yukon Territory and Alaska. *Geomorphology* **67**: 391–406. DOI:10.1016/j.geomorph.2004.11.011

Hinkel KM, Doolittle JA, Bockheim JG, Nelson FE, Paetzold R, Kimble JM, Travis R. 2001. Detection of subsurface permafrost features with ground-penetrating radar, Barrow, Alaska. *Permafrost and Periglacial Processes* **12**: 179–190. DOI:10.1002/ppp.369

Hoekstra P. 1975. Ground and airborne resistivity surveys of permafrost near Fairbanks, Alaska. *Geophysical Research Letters* **40**: 641–656. DOI:10.1190/1.1440555

Jafarov EE, Marchenko SS, Romanovsky VE. 2012. Numerical modeling of permafrost dynamics in Alaska using a high spatial resolution dataset. *The Cryosphere* **6**: 613–624. DOI:10.5194/tc-6-613-2012

Jafarov EE, Romanovsky VE, Genet H, McGuire AD, Marchenko SS. 2013. The effects of fire on the thermal stability of permafrost in lowland and upland black spruce forests of interior Alaska in a changing climate. *Environmental Research Letters* **8**: 035030. DOI:10.1088/1748-9326/8/3/035030

Jepsen SM, Koch JC, Rose JR, Voss CI, Walvoord MA. 2012. Thermal and Hydrological Observations near Twelvemile Lake in Discontinuous Permafrost, Yukon Flats, Interior Alaska, September 2010-August 2011. USGS Open-File Report 2012-1121, 25.

Jepsen SM, Voss CI, Walvoord MA, Minsley BJ, Rover J. 2013a. Linkages between lake shrinkage/expansion and sublacustrine permafrost distribution determined from remote sensing of interior Alaska, USA. *Geophysical Research Letters* **40**: 882–887. DOI:10.1002/grl.50187

Jepsen SM, Voss CI, Walvoord MA, Rose JR, Minsley BJ, Smith BD. 2013b. Sensitivity analysis of lake mass balance in discontinuous permafrost: the example of disappearing Twelvemile Lake, Yukon Flats, Alaska (USA). *Hydrogeology Journal* **21**: 185–200. DOI:10.1007/s10040-012-0896-5

Jiang Y, Rocha AV, Donnell JAO, Drysdale JA, Rastetter EB, Shaver GR, Zhuang Q. 2015. *Journal of Geophysical Research, Earth Surface* **120**: 363–378. DOI: 10.1002/2014JF003180.

Johnstone JF, Chapin FS, Hollingsworth TN, Mack MC, Romanovsky V, Turetsky M. 2010. Fire, climate change, and forest resilience in interior Alaska This article is one of a selection of papers from The Dynamics of Change in Alaska's Boreal Forests: Resilience and Vulnerability in Response to Climate Warming. *Canadian Journal of Forest Research* **40**: 1302–1312. DOI:10.1139/X10-061

Jones HG. 1999. The ecology of snow-covered systems: a brief overview of nutrient cycling and life in the cold. *Hydrological Processes* **13**: 2135–2147.

Jorgenson MT, Romanovsky V, Harden J, Shur Y, O'Donnell J, Schuur EAG, Kanevskiy M, Marchenko S. 2010. Resilience and vulnerability of permafrost to climate change. *Canadian Journal of Forest Research* **40**: 1219–1236. DOI:10.1139/X10-060

Lawson DE, Strasser JC, Strasser JD, Arcone SA, Delaney AJ, Williams C. 1996. Geological and geophysical investigations of the hydrogeology of Fort Wainwright, Alaska Part 1: Canol Road Area. CRREL Report 96-4, 31.

Mckenzie JM, Siegel DI, Rosenberry DO, Glaser PH, Voss CI. 2007. Heat transport in the Red Lake Bog. *Glacial Lake Agassiz Peatlands* **378**: 369–378. DOI:10.1002/hyp

Minsley BJ, Abraham JD, Smith BD, Cannia JC, Voss CI, Jorgenson MT, Walvoord MA, Wylie BK, Anderson L, Ball LB, Deszcz-Pan M, Wellman TP, Ager TA. 2012a. Airborne electromagnetic imaging of discontinuous permafrost. *Geophysical Research Letters* **39**: DOI:10.1029/2011GL050079

Minsley BJ, Smith BD, Hammack R, Sams JI, Veloski G. 2012b. Calibration and filtering strategies for frequency domain electromagnetic data. *Journal of Applied Geophysics* **80**: 56–66. DOI:10.1016/j.jappgeo.2012.01.008

Pastick NJ, Jorgenson MT, Wylie BK, Minsley BJ, Ji L, Walvoord MA, Smith BD, Abraham JD, Rose JR. 2013. Extending Airborne Electromagnetic Surveys for Regional Active Layer and Permafrost Mapping with Remote Sensing and Ancillary Data, Yukon Flats Ecoregion, Central Alaska. *Permafrost and Periglacial Processes* **24**: 184–199. DOI:10.1002/ppp.1775

Pastick NJ, Jorgenson MT, Wylie BK, Rose JR, Rigge M, Walvoord MA. 2014. Spatial variability and landscape controls of near-surface permafrost within the Yukon River Basin. *Journal of Geophysical Research – Biogeosciences* **119**: 1244–1265. DOI:10.1002/2013JG002594

Prowse TD, Impacts C, Columbia B, Brown K. 2010. Appearing and disappearing lakes in the Arctic and their impacts on biodiversity. 68–70.

Riseborough D, Shiklomanov N, Etzemuller S, Gruber S, Marchenko S. 2008. Recent Advances in Permafrost Modelling. *Permafrost and Periglacial Processes* **156**: 137–156. DOI:10.1002/ppp

Schultz GM, Ruppel C. 2005. Inversion of inductive electromagnetic data in high induction number terrains. *Geophysics* **70**: G16–G28.

Schuur EAG, McGuire AD, Schädel C, Grosse G, Harden JW, Hayes DJ, Hugelius G, Koven CD, Kuhry P, Lawrence DM, Natali SM, Olefeldt D, Romanovsky VE, Schaefer K, Turetsky MR, Treat CC, Vonk JE. 2015. Climate change and the permafrost carbon feedback. *Nature* **520**: 171–179. DOI:10.1038/nature14338

Shiklomanov N, Nelson F. 1999. Analytic representation of the active layer thickness field, Kuparuk River Basin, Alaska. *Ecological Modelling* **123**: 105–125. DOI:10.1016/S0304-3800(99)00127-1

Shur Y, Hinkel KM, Nelson FE. 2005. The transient layer: implications for geocryology and climate-change science. *Permafrost and Periglacial Processes* **16**: 5–17. DOI:10.1002/ppp.518

Shur YL, Jorgenson MT. 2007. Patterns of Permafrost Formation and Degradation in Relation to Climate and Ecosystems. **19**: 7–19. DOI: 10.1002/ppp.

Tikhonov AN. 1953. Solution of incorrectly formulated problems and the regularization method. *Soviet Meth. Dokl.* **4**: 1035–1038.

Watanabe K, Kito T, Wake T, Sakai M. 2011. Freezing experiments on unsaturated sand, loam and silt loam. *Annals of Glaciology* **52**: 37–43. DOI:10.3189/172756411797252220

Wellman TP, Voss CI, Walvoord MA. 2013. Impacts of climate, lake size, and supra- and sub-permafrost groundwater flow on lake-talik evolution, Yukon Flats, Alaska (USA). *Hydrogeology Journal* **21**: 281–298. DOI:10.1007/s10040-012-0941-4